Article

The International Journal of
Robotics Research
2015, Vol. 34(14) 1731–1746

DOI: 10.1177/0278364915608250
ijr.sagepub.com

Dimensional synthesis of three-fingered robot hands for maximal precision manipulation workspace

Júlia Borràs and Aaron M. Dollar

Abstract

This paper applies dimensional synthesis to explore the geometric design of dexterous three-fingered robotic hands for maximizing precision manipulation workspace, in which the hand stably moves an object with respect to the palm of the hand, with contacts only on the fingertips. We focus primarily on the tripod grasp, which is the most commonly used grasp for precision manipulation. We systematically explore the space of design parameters, with two main objectives: maximize the workspace of a fully actuated hand and explore how under-actuation modifies it. We use a mathematical framework that models the hand-plus-object system and examine how the workspace varies with changes in nine hand and object parameters such as link length and finger arrangement on the palm.

Results show that to achieve the largest workspaces the palm radius should be approximately half of a finger length larger than the target object radius, that the distal link of the two-link fingers should be around 1–1.2 times the length of the proximal link, and that fingers should be arranged symmetrically about the palm with object contacts also symmetric. Furthermore, a proper parameter design for an under-actuated hand can achieve up to 50% of the workspace of a fully actuated hand. When compared to the system parameters of existing popular hand designs, larger palms and longer distal links are needed to maximize the manipulation workspace of the studied design.

Keywords

Multi-fingered hands, dimensional synthesis, hand workspace, dexterous manipulation

1. Introduction

Robotic and prosthetic hand designers have been interested in replicating the functionality of the human hand for many decades. The human hand accomplishes both dexterous within-hand manipulation and robust grasping, but with more than 21 joints and complex tendon routing (Bullock et al., 2012b; Grebenstein et al., 2010; Martell and Gini, 2007; Matsuoka et al., 2006) . Nevertheless, simpler hands with fewer joints and fingers can still achieve a high degree of functionality with a simplified structure as shown by Mason and Salisbury (1985); Mason et al. (2011); Townsend (2000); Salisbury and Craig (1982); and Schunk (2013). However, there is considerable research to be done to achieve extra functionality beyond power-grasping with simplified hands. In this paper, we examine the design of a common three-fingered arrangement, the tripod grasp (Bullock et al., 2013; Cutkosky, 1989) (Figure 1, top), for the purposes of maximizing the workspace over which a grasped object can be repositioned in static equilibrium and without breaking contact, i.e. precision manipulation (Bullock et al., 2012a; Kerr and Roth, 1986) (Figure 1, bottom). We show that smart design choices and informed parameter optimization are needed to avoid important workspace reductions.

There have been many research efforts to examine the design parameters of robotic hands and how they affect grasping performance, e.g. Ciocarlie and Allen (2011); Ciocarlie et al. (2013); Hammond et al. (2012); Shimoga (1996). However, very few previous works have specifically examined the design of fingered hands for the purposes of large precision manipulation workspaces. Notable exceptions include the Okada Hand (Okada, 1982), Utah/MIT Hand (Jacobsen et al., 1986), with precision manipulation demonstrations by Michelman (1998), the Stanford/JPL Hand (Mason and Salisbury, 1985; Salisbury and Craig, 1982), the DLR Hands (Butterfaß et al., 1998, 2001;

Mechanical Engineering and Materials Science, Yale University, USA

Corresponding author:
Julia Borras Sol, Mechanical Engineering and Materials Science, Yale University, New Haven, CT 06520, USA.
Email: julia.borrassol@kit.edu

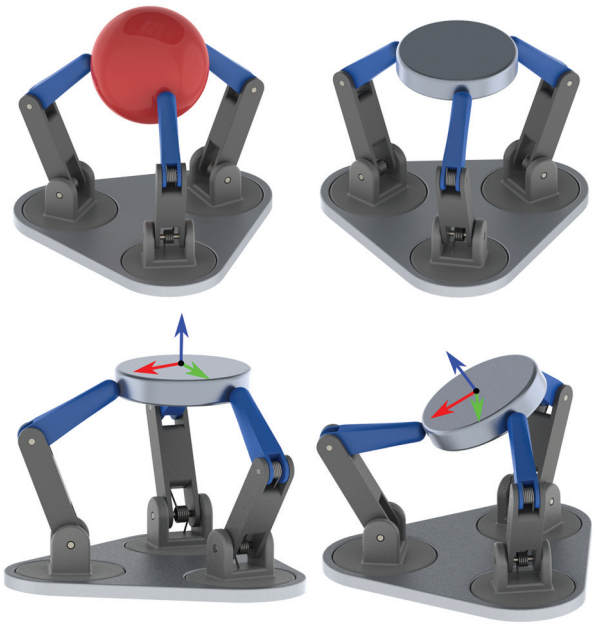

Fig. 1. Top: A simple three-fingered hand doing two tripod precision grasps. Bottom: Two in-hand object poses. We want to explore how to optimize the geometry of the hands to maximize the number of in-hand object poses that can be achieved during in-hand manipulation without breaking contact.

Grebenstein et al., 2011), and the Metahand (Dai et al., 2009). However, researchers have yet to thoroughly examine how the detailed design parameters of a hand, including the finger and palm kinematics, can be synthesized in order to maximize the precision manipulation workspace of the hand grasping a range of objects held within the fingertips.

In this paper we examine the dimensional synthesis of a common class of three-fingered grasp for the purposes of investigating how variations in design parameters affect the precision manipulation capabilities, and in particular the range of positions and orientations over which a circular object held within the fingertips can be stably positioned. This class of three-fingered grasp, with two links per finger, covers many popular architectures of robotic hands such as the Barrett hand (Townsend, 2000), the IPR SCHUNK Dexterous Hand SDH-2 (Schunk, 2013) and the iRobot-Harvard-Yale (iHY) Hand (Odhner et al., 2013), and it is similar to many other three-fingered hands such as the JPL hand (Salisbury and Craig, 1982).

A second objective of the paper is to investigate how under-actuated transmissions can modify the size of the manipulation workspace. Under-actuated hands achieve an open-loop adaptive behavior that has proved to be very successful for power-grasping a wide variety of objects in unstructured environments (Dollar and Howe, 2010). However, such advantages come at an expense of reducing the dimension of the wrench space that can be realized at the fingertips, therefore reducing the manipulation workspace. We will quantify the reductions and show how design parameters can greatly minimize such reduction. We will also show how design parameters that lead to maximal workspaces for fully actuated hands do not necessary lead to the maximal size for an under-actuated version of the same hand.

Dimensional synthesis involves the study of the proper dimensions of a given mechanism design to improve its performance. It is well known that a manipulator with well-designed dimensions will exhibit overall better performance than one designed intuitively but with poorly chosen dimensions. However, because of the complexity of the hand structure and the high coupling between different characteristics that condition its performance, dimensional synthesis of robotic hands has not been widely applied. One of the first to apply it to robotic hands was Salisbury and Craig (1982). They studied how to design fingers to avoid singularities and applied a numerical approach to define its optimal dimensions. In contrast, we will analyze the hand-plus-object and its properties as a whole using a mathematical framework from parallel manipulators adapted to robotic hands (Borràs and Dollar, 2013b, 2013a, 2014), using screw theory similarly as done in works such as Cui and Dai (2012). The parallelism between parallel robots and grasping has been used before to define dexterity measures for grasping (Bicchi and Prattichizzo, 2000). In previous work we showed how two parameters related to the compliance and tendon pulling of the fingers can greatly increase the size of the manipulation workspace of an under-actuated hand of a specific design (Borràs and Dollar, 2013b, 2014). In this work, we explore a bigger set of parameters for fully actuated and under-actuated hands, including the geometry of the fingers, the palm and its symmetry, in combination with other parameters such as compliance and the transmission ratio that appear in under-actuated hands.

This paper is organized as follows. First a discussion is given of the general dimensional synthesis approach taken in this paper, and then the mathematical formulation of the problem is presented. The following section outlines the methodology for computing systematically the workspaces and calculating their size. The results of our computations are presented and finally a discussion of the results and some conclusions are given.

2. Dimensional synthesis approach

We proved in previous works that the hand we want to examine has the same structure as a parallel manipulator when it is holding an object with its fingertips (Borràs and Dollar, 2013a). Therefore, mathematical frameworks commonly used for parallel manipulators can be used to model the hand, adapted to include friction and contact constraints (Borràs and Dollar, 2013b, 2014) . As a result, both fields can benefit of mutual transfer of knowledge. In particular, in this paper we are interested in exploring dimensional synthesis results in parallel robots to be applied to robotic hands.

Indeed, the field of parallel manipulators has extensively explored dimensional synthesis. Jean-Pierre Merlet defines four different main approaches (Merlet, 2006a).

1. *The atlas approach*. This reduces the number of parameters to a small set and then it defines measurements for all the combinations, showing the results as a graphical representation where the optimal can be chosen visually.
2. *The cost function approach*. This defines a cost function with a weighted sum of indexes that need to be optimized, finding the design parameters that optimize it using numerical techniques.
3. *The exact synthesis approach*. This optimizes for a particular task, defined as a set of poses, velocities, and accelerations. It solves analytically the design parameters whose workspace includes the prescribed poses.
4. *The parameter space approach*. This defines a space where each dimension represents a design parameter. Each design requirement corresponds to an area of such space, and several requirement areas can be intersected. The optimal geometry search, for a solution that holds several requirements, can be done searching only in the intersection.

The second approach is by far the most widely used in the context of parallel manipulators, but often with a single index optimization that does not take into account other requirements (Merlet, 2006a; Tsai, 1999). Defining a weighted sum of different indexes is often arbitrary and, therefore, their results can be misleading (Das and Dennis, 1997). In addition, it has already been proved in the context of parallel robots that manipulability indexes or condition numbers do not define a proper measure of quality (Merlet, 2006b), and therefore any cost function relying on those indexes can be also misleading. In conclusion, although the cost function approach could be directly applied to robotic hands, it does not seem promising because, in addition to the mentioned drawbacks, for robotic hands we need to consider additional restrictions such as contact friction constraints and fingers that can only push and not pull.

The third approach becomes unwieldy when dealing with complex geometries. It has been applied for single-finger design (Dai and Wang, 2007), and also for structures that take into account several fingers (Simo-Serra et al., 2012). However, it implies the resolution of very complex systems of equations and solutions are optimal only for very specific tasks that specify a discrete number of configurations and velocities in the workspace.

The first approach allows the exploration of the entire parameter space and therefore, it guarantees a global optimum. However, the need of presenting results graphically limits this approach to the exploration of only 2 or 3 parameters. The generalization of this concept leads to the fourth approach, where several requirements can be intersected.

For the present work, we suggest a combination of the first and the fourth approach. We propose a novel graphical representation of parameter spaces with more than three dimensions as polygons with as many vertexes as parameters. Despite the simplicity of the approach, it allows taking into account joint limits, friction cone conditions, and avoidance of singularities, as the other approaches do.

As in all optimization methods, we need to establish assumptions to reduce the parameter exploration space. In our case, on the shape of the object we assume the normal to the object surface at the contact points directed towards the center of mass. That is valid for spheres, discs, and other round objects, which are the most commonly grasped with tripod grasps. We also fix the structure of links and joint axis orientations. However, our results give insights to a wide range of existing hand designs and our methods could be easily applied to other designs. Finally, we focus on the maximization of the size of the workspace, not its shape, or its properties. Properties such as manipulability can also be included, and are analyzed in the last section of the paper.

In practice, a design process should take into consideration combined criteria including grasping and workspace. Nevertheless, this work is useful to show how optimal parameters for workspace size are significantly different from parameters for other criteria. Indeed, we show how, if the size of the workspace is ignored, particularly for underactuated hands, the resulting design could have a much-reduced workspace that could greatly limit the versatility of the designed hand.

3. Mathematical formulation

Consider the hand-plus-object system formed by the three-fingered hand (with two-link fingers), the contact points, and the object shown in Figures 1 and 2. Each finger i has three rotational joints with axis z_{i1}, z_{i2} and z_{i3} ($z_{i2} \parallel z_{i3}$ and $z_{i1} \perp z_{i2}$) as shown in Figure 2, written with respect to a fixed reference frame located at the palm, with angles of rotation θ_{i1}, θ_{i2}, and θ_{i3}, respectively. The 0 angle configuration corresponds to a full opened hand with the fingers equally spread around the palm. The position and orientation of the object with respect to the palm reference frame are given by a position vector $\boldsymbol{p} \in \mathbb{R}^3$ of the center of mass (CoM) of the object and a rotation matrix $\boldsymbol{R} \in SO(3)$, together forming the object local reference frame $\{\boldsymbol{p}, \boldsymbol{R}\}$. Therefore, the object workspace is 6-dimensional. Given the object pose, if the locations of the contact points in the object reference frame are given by the position vectors $\tilde{\boldsymbol{c}}_i$, we can transform them to the global reference frame as

$$\boldsymbol{c}_i = \boldsymbol{p} + \boldsymbol{R}\tilde{\boldsymbol{c}}_i \tag{1}$$

The total number of joints of the hand is $m = 9$. We represent each contact point on the object as three additional passive joints, acting as a spherical joint that is free to move. This is locally equivalent to the point contact with

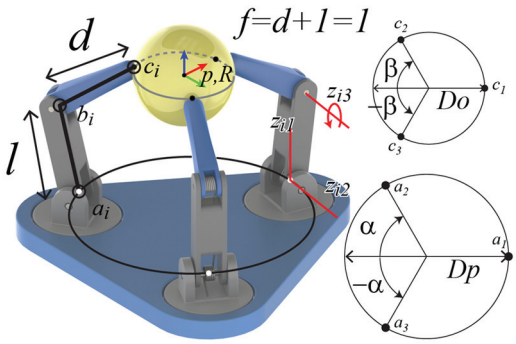

Fig. 2. Model of the studied hand (top) with its design parameters.

friction contact model (Borràs and Dollar, 2013a). Therefore, the total number of joints of the hand-plus-object system is $m+9$. Let

$$\mathbf{q} = (\theta_{11}, .., \theta_{33})^T \tag{2}$$

be the 9-dimensional vector of all the hand joint angles. Any value of $\mathbf{q}$ determines a configuration of the hand, but once the object is grasped, only six joint angles are independent and determine the position of the object, and the rest are determined by contact constraints, namely, the fingertip contact points must remain in contact with the object at the same contact points during the in-grasp manipulation.

In our approach, we will sample the position and orientation space of the object. Each object pose determines the location of the contact points through equation (1) that are used to solve the inverse kinematics of each finger to obtain the corresponding configuration of the hand. Details on how to solve the kinematics can be found in Borràs and Dollar (2013b).

3.1 Fully actuated hand static equilibrium equations

There are several approaches to define the matrix that maps the joint velocities $\dot{\mathbf{q}}$ to the platform/object 6-dimensional twist $\boldsymbol{v}$ (Tsai, 1999). Here we will use the theory of reciprocal screws using the framework presented in Borràs and Dollar (2014), that is based on a parallel robot framework (Mohamed and Duffy, 1985). The matrix $\boldsymbol{J}$ is called the Jacobian matrix of the system, and defines the linear relationship between the object twist and the velocities at the joints as

$$\boldsymbol{J}\boldsymbol{v} = \dot{\mathbf{q}} \tag{3}$$

It is well known that the same matrix, transposed, describes the mapping between external transmitted wrench on the object and the torques exerted at the joints. Then, if $\boldsymbol{w}$ is the total external 6-dimensional wrench acting on the object, and $\boldsymbol{\tau}$ is the 9-dimensional vector of torques exerted by each joint, we can write

$$-\boldsymbol{w} = \boldsymbol{J}^T\boldsymbol{\tau} \tag{4}$$

For the studied manipulator, the Jacobian is a 6×9 matrix expressed as $\boldsymbol{J}^T = (\cdots \boldsymbol{s}_{i1}\ \boldsymbol{s}_{i2}\ \boldsymbol{s}_{i3}\cdots)$, for $i=1,2,3$, where each column $\boldsymbol{s}_{ij}$ is the 6-dimensional jth wrench of the finger i, and they are of the form

$$\boldsymbol{s}_{ij} = (\boldsymbol{g}_{ij}, \boldsymbol{h}_{ij}) \tag{5}$$

where $\boldsymbol{g}_{ij}$ corresponds to the force part of the wrench, and $\boldsymbol{h}_{ij}$ the rotational-moment part.

Equation (4) defines the static equilibrium of the hand-plus-object. From equations (4) and (5) we can rewrite the fingertip forces with respect to the palm reference frame as

$$\boldsymbol{f}_i = \sum_{j=1}^{3} \tau_{ij}\boldsymbol{g}_{ij}, i=1,2,3 \tag{6}$$

This fingertip force ignores the rotational part of the wrenches (the moment) because with the point with friction model, the moments are not transmitted to the object.

A configuration can only be considered inside the manipulation workspace if it is in static equilibrium and the corresponding fingertip forces are inside the friction cones.

To check the friction cone conditions, we need some information about the object. As we mentioned, we assume the vector normal to the plane tangent to the surface of the object at the contact normal to be directed towards the center of mass, located at $\boldsymbol{p}$. Therefore, it can be defined as $\boldsymbol{n}_i = \boldsymbol{p} - \boldsymbol{c}_i$, where $\boldsymbol{c}_i$ is the contact point. The fingertip force obtained in equation (6) is then inside the friction cone if the projection on that normal vector ${}^n f_i = \boldsymbol{n}_i^T\boldsymbol{f}_i$, and the projection on the normal plane to the vector, ${}^\perp f_i = ||\left(\boldsymbol{Id} - \boldsymbol{n}_i\boldsymbol{n}_i^T\right)\boldsymbol{f}_i||$ satisfy

$${}^\perp f_i \le \mu {}^n f_i \tag{7}$$

where μ is the coefficient of friction and is taken as 0.7 for the executions.

Note that the formulation introduced so far is general and can be applied to any hand following results in Borràs and Dollar (2014).

3.2 Under-actuated hand static equilibrium equations

When using under-actuated fingers, there are more joints than actuators. Many of the latest under-actuated hands use tendon cables combined with compliant joints (Dollar and Howe, 2010; Odhner et al., 2013) as in Figure 3 . For these hands, we can model the transmission mechanism as a coupling between the torques exerted by the joints actuated by the same cable. Following results in Balasubramanian et al. (2012), assuming that the tendon remains in contact with the pulley, and the pulley radii are constant, such coupling depends only on the ratio between the radii of the pulleys, which we call the transmission ratio T_r.

We consider the second and third joints of each finger i (with axes of rotation z_{i2} and z_{i3} in Figure 2) to be compliant and actuated by the same pulling cable, as the two joints in the finger of Figure 3, while the first joints of the fingers are independently actuated. As shown in Figure 3, there is a pulling cable and torsion springs in parallel with each of the joints. Therefore, the torque exerted by each of these joints can be decomposed into the torque exerted by the cable plus the one done by the spring according to Hooke's law:

$$\tau_{ij} = {}^{a}\tau_{ij} - k_j(\theta_{ij} - \delta_j) \tag{8}$$

for each finger $i = 1, 2, 3$ and joint $j = 2, 3$, where $k_j > 0$ is the spring stiffness constant of the jth joint spring in each finger i and δ_j is its resting configuration angle. Note that $k_1 = 0$. Note also that this expression can be expressed for any hand with any tendon routing configuration.

For a given configuration and a given external applied force, substituting (8) into the system in (4) leads to a linear system where the unknowns are the nine actuation torques

$$-\boldsymbol{w} = \boldsymbol{J}^{T\,a}\boldsymbol{\tau} + \boldsymbol{J}^{T\,c}\boldsymbol{\tau} \tag{9}$$

where we have split the vector of torques into the actuation torques ${}^{a}\boldsymbol{\tau} = ({}^{a}\tau_{ij})$ and the compliant torques ${}^{c}\boldsymbol{\tau} = (-k_j(\theta_{ij} - \delta_j))$. As the actuation torques exerted by the same cable only depend on the radius of the pulley, they are proportional, and we can write ${}^{a}\tau_{i3} = T_r\,{}^{a}\tau_{i2}$, where T_r is the ratio between the radius of the third joint pulley and the radius of the second joint pulley. Thus, we can rewrite ${}^{a}\boldsymbol{\tau}$ as a 6-dimensional vector, and the above system can be rewritten as

$$-\boldsymbol{w} = \boldsymbol{J}_a^{T\,a}\boldsymbol{\tau} + \boldsymbol{J}^{T\,c}\boldsymbol{\tau} \tag{10}$$

where $\boldsymbol{J}_a^T$ is a 6×6 matrix obtained from $\boldsymbol{J}^T$ combining the columns as

$$\boldsymbol{J}_a^T = (\cdots, \boldsymbol{s}_{i1}, \boldsymbol{s}_{i2} + T_r\boldsymbol{s}_{i3}, \cdots) \tag{11}$$

Note that a solution of the system would represent a valid configuration only if the cables were exerting a positive force. Depending on the routing of the cable, the tendons always exert torque of the same sign; in this case, we choose it to be positive.

In conclusion, when computing the workspace, we consider a configuration to be inside the kinematic workspace if it satisfies the following conditions.

1. The position and orientation of the object lead to a real inverse kinematic solution.
2. The flexion finger joint angles are between 0 and 90°.
3. The angle between the vectors $\boldsymbol{c}_i - \boldsymbol{b}_i$ (following the contact phalange) and the vector normal to the object surface at the contact point is larger than 120°. We consider this restriction because we are approximating a rolling contact with a point contact, which only holds locally, i.e., close to a chosen home configuration.

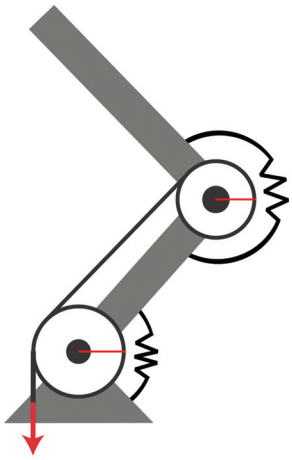

Fig. 3. Simple scheme of an under-actuated finger using tendon cables that cross multiple passive compliant joints. The pulley radii are shown in red.

If all the joints are actuated, as in a fully actuated hand, the static equilibrium equations in (4) have a 3-dimensional solution, and therefore, in a generic configuration, there is always a solution that satisfies (7), assuming that we don't limit the actuation torques values. Therefore, all the configurations in the kinematic workspace are theoretically part of the manipulation workspace of the fully actuated version of the hand.

On the contrary, for the under-actuated version of the hand, only a 0-dimensional solution of the static equilibrium equations exists. Therefore, not all the configurations in the kinematic workspace will be feasible. In other words, in addition to the previous conditions, a configuration is considered to be inside the manipulation workspace of the under-actuated version of the hand if:

(a) it satisfies static equilibrium equations (10);
(b) the corresponding fingertip forces are inside the friction cones; and
(c) the actuation torques exerted by the tendon cables are positive.

To obtain the overall maximum without falling into local minima, we explore all possible configurations of the hand-plus-object according to a given 6-dimensional discretized space of poses for the object (Figure 4), and for a given external applied force. If for a configuration and a force there is a solution of the static equilibrium equations that satisfy the conditions (a) to (c) listed above, it means that the configuration belongs to the manipulation workspace of the under-actuated hand. Also, we simplify further the problem considering only forces of magnitude 0. In this situation, the actuation torques are still not zero as they need to compensate for the force done by the compliant joints, and results are valid for external forces of small magnitudes in any possible direction.

Finally, we want to note that we do not study how to control the hand to move from one configuration to another. However, transitions from one point to another are possible,

and could be obtained using an energy minimization problem as suggested in Odhner and Dollar (2011).

For the simulations in this work, we do not limit the torque the motors can exert, but we do discard singular configurations. These are configurations in which the Jacobian matrix is very close to being rank deficient, and we cannot solve the linear system in (10). In the field of parallel robots, singularities have been widely studied, for details, see Gosselin and Angeles (1990). For configurations closer to a singularity, the magnitude of the torques can grow infinitely and thus, in practice, the size of the manipulation workspace can be limited by this factor. However, for fully actuated hands usually a solution can be found with minimized torques, and for under-actuated hands we will see how we can reduce the exerted torques by modifying some of the stiffness constants without modifying the direction of the fingertip forces, and thus, without modifying the size of the manipulation workspace.

4. Methodology

We distinguish two types of parameters: geometric parameters and manipulation parameters. The first group defines the geometry of the hand and they are sufficient to compute the kinematic workspace defined by just solving the kinematics. This is enough to compute the workspace of fully actuated hands. The second group is related to compliance and transmission ratios parameters that are necessary to compute the workspace of the under-actuated hand.

To normalize the results across different hand sizes we consider a fixed finger length of 1, and we define ratios of parameters for this fixed finger length (Figure 2 and Table 1). (Note, this paper omits the units because they are not relevant for the method. By default, consider ISU: meter (m), radian (rad) and Newton (N). The results are scalable to any hand size desired.). The parameters described in Table 1 are:

1. $\mathrm{P_r}$ Ratio between the diameter of the palm and the length of the finger.
2. O_r Ratio between the diameter of the object and the length of the finger.
3. $DP_r = d/l$ Ratio between distal (d) and proximal (l) link lengths. Because we fix $d + l = 1$, it is equivalent to give values to the proximal link length l instead.
4. α : Angle (in rad) of polar coordinates for the palm finger attachments $\boldsymbol{a}_2$ and $\boldsymbol{a}_3$ (see Figure 2).
5. β: Angle (in rad) of polar coordinates for the contact points $\boldsymbol{c}_2$ and $\boldsymbol{c}_3$ (see Figure 2).

The two angle parameters encode the symmetry of the hand, being symmetric with respect to all fingers when $\alpha = \beta = \pi/3$. Note that the geometrical parameters above are enough to solve the kinematics.

The manipulation parameters are:

Table 1. Design parameters.

Parameter	Def.	Range
P_r	D_p/f	$(1, 2.5)$
DP_r	d/l	$(0.4, 2.3)$
O_r	D_o/f	$(0.3, 1.5)$
α		$(\pi/6, \pi/2)$
β		$(\pi/6, \pi/2)$
K_r	k_3/k_2	$(0.5, 4)$
T_r	r_3/r_2	$(0.6, 1.2)$

(a) $K_r = k_3/k_2$ stiffness constants ratio between the third and the second joint springs;
(b) k_2 stiffness constant of second joint springs;
(c) T_r transmission ratio, i.e., ratio between the pullies radii of the third and second joints;
(d) δ_2 and δ_3: resting configurations of the springs.

We are considering cables pulling in an active close mechanism, hence we set the two resting configuration angles of the springs to 0, so that the resting configuration is the hand opened. We also consider a null external force. Then, we can rewrite the static equilibrium equations (10) as

$$-k_2\, \boldsymbol{J}^T \begin{pmatrix} \boldsymbol{K}_1 & 0 & 0 \\ 0 & \boldsymbol{K}_2 & 0 \\ 0 & 0 & \boldsymbol{K}_3 \end{pmatrix} \boldsymbol{q} = \boldsymbol{J}_a^T\, {}^a\boldsymbol{\tau} \tag{12}$$

where K_i are the stiffness matrices of each finger and have the form

$$\boldsymbol{K}_i = \begin{pmatrix} 0 & 0 & 0 \\ 0 & 1 & 0 \\ 0 & 0 & K_r \end{pmatrix}$$

and $\boldsymbol{q}$ is the vector of joint angles defined in (2).

From system (12) we can state that the actuation torques ${}^a\boldsymbol{\tau}$ are proportional to k_2. In addition, from equation (6) we can write the fingertip force as

$$\begin{aligned} &\boldsymbol{f}_i = \tau_{i1}\boldsymbol{g}_{i1} + \tau_{i2}\boldsymbol{g}_{i2} + \tau_{i3}\boldsymbol{g}_{i3} = \\ &({}^a\tau_{i1}\boldsymbol{g}_{i1} + \left({}^a\tau_{i2} + k_2\theta_{i2}\right)\boldsymbol{g}_{i2} + \left(T_r\,{}^a\tau_{i2} + K_r k_2 \theta_{i3}\right)\boldsymbol{g}_{i3} = \\ &{}^a\tau_{i1}\boldsymbol{g}_{i1} + {}^a\tau_{i2}(\boldsymbol{g}_{i2} + T_r\boldsymbol{g}_{i3}) + k_2(\theta_{i2}\boldsymbol{g}_{i2} + K_r\theta_{i3}\boldsymbol{g}_{i3}) \end{aligned} \tag{13}$$

As before, we concluded that the actuation torques, ${}^a\tau_{i1}$ and ${}^a\tau_{i2}$, are all proportional to k_2, the last expression in (13) is proportional to k_2, and so, we can conclude that fingertip forces are proportional to k_2. In other words, when no external force is considered, the parameter k_2 only modifies the magnitude of the fingertip forces, but not their direction. Note that this is not true under the presence of an external force, but in our case it allows us to remove k_2 from the parameter space. Results are orientative and valid for small external forces. In addition, the value of k_2 can also be used to reduce the mangitude of the actuation

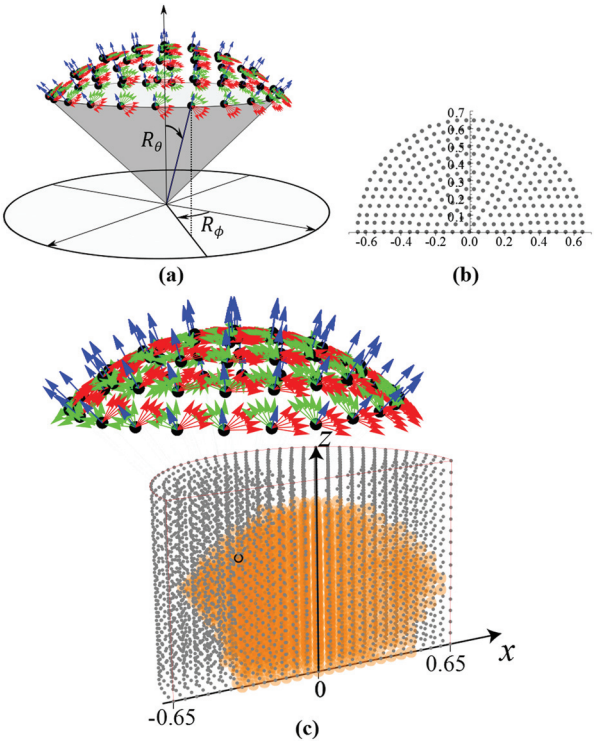

Fig. 4. (a) Discretization for orientations. Each red-green-blue set represents the orientation of the object reference frame, as in the two examples in Figure 1-bottom (b) Discretization for positions X–Y. The ranges and intervals of discretization for position and orientations are shown in Table 2. Note that the interval for R_ϕ depends on a parameter r that codifies how far away you are from $R_\theta = 0$. (c) Combination of position and orientation discretization. For each position, we consider the set of orientations in (a). We also show an example of position workspace in orange.

torques. As we are interested in small actuation torques, we set $k_2 = 0.5$.

4.1 Discretization of the workspace

We consider a discretization of the workspace in position and orientation. Each kinematic workspace will be a subset of all the configurations and each manipulation workspace of the under-actuated hand version a subset of the kinematic workspace. The chosen discretization is shown in Table 2 and Figure 4. The step in x and z is 0.05 and the positions are distributed radially as in Figure 4(b). (Again, we omit units because it is all scalable according to the size of the finger. Using the ISU, that would be 0.05 m for a 1 m finger.) The orientations are sets of rotation matrices $\boldsymbol{R} = (\boldsymbol{i}, \boldsymbol{j}, \boldsymbol{k})$, where vectors $\boldsymbol{k}$ (in blue in the figure) represent the vector normal to the plane formed by the three contact points, and they are distributed around a sphere that represents the span of orientations around OX and OY (Figure 4(a)). For the discretization used, a total of 4,879 positions are combined with 305 orientations at each position, leading to $1,488,095$ object poses. The range of motion considered for each pose parameter is shown in Table 2.

Table 2. Discretization parameters.

	Range	Interval
x, y	$(-0.65, 0.65)$	0.05
z	$(0.2, 1)$	0.05
R_z	$(-\pi/6, -\pi/6)$	$\pi/12$
R_θ	$(-\pi/4, \pi/4)$	$\pi/16$
R_ϕ	$(0, \pi)$	$\frac{2\pi}{(r+1)6}$

We define the size of the workspace by simply counting the number of configuraitons inside the workspace. As we are only interested in choosing the parameters with bigger workspace, we do not need to define a proper volume, but just compare between different sizes.

We are looking for the biggest workspace, and therefore we want to know if the discretization of our workspace is affecting at the order in size of different computed hand workspaces. To study this, we computed the size of the kinematic workspaces of 20 well-distributed different geometries of hands using six different discretizations, described in the table in Figure 5 (top). Each discretization increases the number of object poses, with number 6 being the most accurate one with a total of more than 29 million poses.

For each discretization, we computed the size of each workspace and divided its value by the biggest one, so that for each discretization, we have a list of sizes for each of the 20 hands that range from 0 to 1:

$$disc_i = \{{}^i ws_1, \ldots, {}^i ws_{20}\}, i = 1, \ldots, 6$$

Note that in each list $disc_i$ at least one value is 1. The values obtained for the most accurate discretization, $disc_6$, were the closest to the truth, and so, we compared all the rest to them:

$$disc_i = \{{}^i ws_1 - {}^6 ws_1, \ldots, {}^i ws_1 - {}^6 ws_{20}\}, i = 1, \ldots, 5$$

Figure 5 (bottom) shows the mean values of the above values for each discretization. In other words, the bars represent the mean differences in size for all of the 20 hands. We can see that for the used discretization, the obtained erros are, at the maximum, only 0.03 (that is, the workspace sizes are 3% different than sizes computed with discretization number 6), and the mean difference is only 1% (indicated by the dashed line in the graphic). Therefore, for the results shown in the next section, we always consider as optimal the best 2% sizes.

5. Results

We considered first the full actuated hand and we swept all the geometric parameters: palm, distal–proximal ratio, and the size of the object. The length of the fingers is fixed,

$l + d = 1$; therefore, the range shown for DP_r corresponds to lengths of the proximal link from 0.3 to 0.7.

Using the discretization selected in the previous section, we checked the 1,488,095 possible configurations for each combination of geometric design parameters for the ranges shown in the Table 1. The obtained 2% maximum size of the workspaces for a fully actuated hand is 124,451 and 122,914 configurations. The maximum sizes are obtained with the geometrical parameters

$$\{P_r = 1.5,\ l = 0.4,\ O_r = 0.3\},\ \text{and}$$
$$\{P_r = 1.25,\ l = 0.4,\ O_r = 0.3\} \tag{14}$$

respectively.

Figure 6 (top) shows the evolution of workspace size when the geometric parameters change for different object sizes. The color bar on the left represents the evolution of the fully actuated workspace size, from the biggest size obtained with dark color (124,451 configurations) to 0 configurations (light color). The figure shows that, when the object size increases, we can observe that palm size increases accordingly, whereas the optimal proximal link length slightly decreases.

We performed a similar simulation computing the size of workspaces for the under-actuated hand defined in the previous section, using the sweeping of the same geometric parameters, and adding the sweeping of T_r from 0.6 to 1.2, and fixing $K_r = 4$. Figure 6 (bottom) shows the results following the color bar on the right from the maximum obtained size in dark color (52,441) to 0 with light color.

From Figure 6 we can observe that the optimal trends for palm-object sizes are similar for fully and under-actuated hands. However, the sizes of the fully actuated hand workspaces are big consistently for wide ranges of the proximal link length, while the proximal link length needs to be close to 0.5 for under-actuated hands, independently of the transmission ratio used.

Table 3 shows the results of the 10 best fully actuated workspaces. The table contains also the maximal under-actuated hand workspace that can be achieved with each corresponding geometrical parameter and the manipulation parameters needed to obtain it. The last column shows the percentage of the fully actuated hand workspace that is part of the under-actuated hand workspace. We can see that using under-actuation implies a reduction between 80 to 50% of the workspace. However, our computations indicate that the lost configurations are always located at the border, away from the inside/central configurations, which are in practice most likely to be part of feasible workspace when taking into account rolling contacts and motor torque limits.

Table 3 also tells us that the biggest size of under-actuated hand workspace does not coincide with the optimal for the fully actuated hand. Indeed, with the optimum geometric parameters ($P_r = 1.5$, $l = 0.4$, $O_r = 0.3$) the maximum feasible workspace that can be obtained with under-actuation is only 36,035 configurations, with $T_r = 0.8$,

	Step x,z	# Positions	# Orientations	Total # of poses
1	0.07	1,740	111	193,140
2	0.07	1,740	305	530,700
3	0.05	4,879	111	541,569
Used	0.05	4,879	305	1,488,095
4	0.03	19,305	305	5,888,025
5	0.05	4,879	1,519	7,411,201
6	0.03	19,305	1,519	29,324,295

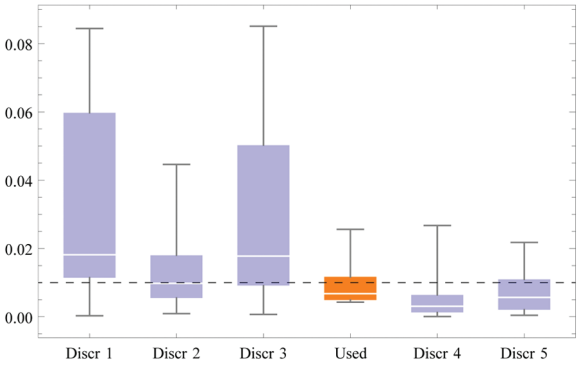

Fig. 5. Table with different workspace discretizations and the mean errors obtained when computing the size of the workspaces compared to the sizes obtained using the sixth optimization (with 29 million configurations).

but the size of the biggest under-actuated workspace is 45.5% bigger. This is an important result, because it shows us that for an optimal size of workspace for an under-actuated hand, it is not enough to use an optimal fully actuated hand, but an independent optimization needs to be computed.

Therefore, we run an independent simulation by sweeping all the parameters in the ranges shown in the Table 1, including the stiffness ratio, but fixing α and β at $\pi/3$ (for a symmetric hand with respect to each finger), to compute the sizes of the under-actuated hand workspaces.

We computed a total of 6,125 workspaces. The 2% maximum obtained workspaces for the under-actuated hand contain 52,441 and 52,321 configurations and they are obtained with the parameters

$$\{P_r = 1.25,\ l = 0.5,\ O_r = 0.3,\ K_r = 4,\ T_r = 0.8\}\ \text{and}$$
$$\{P_r = 1.25,\ l = 0.5,\ O_r = 0.3,\ K_r = 4,\ T_r = 0.9\} \tag{15}$$

respectively.

The results are plotted in Figure 7. To be able to plot the five dimensions of the parameter space, we plot a polygon for each set of data (parameters, size), where each polygon vertex corresponds to the value of the parameter and the color code represents the size of the workspace, compared to the biggest one, and thus, ranging from 0 to 100. In additon to the five parameters, each polygon has two extra vertexes that correspond to the coordinates x and z of the centroid of the computed workspace.

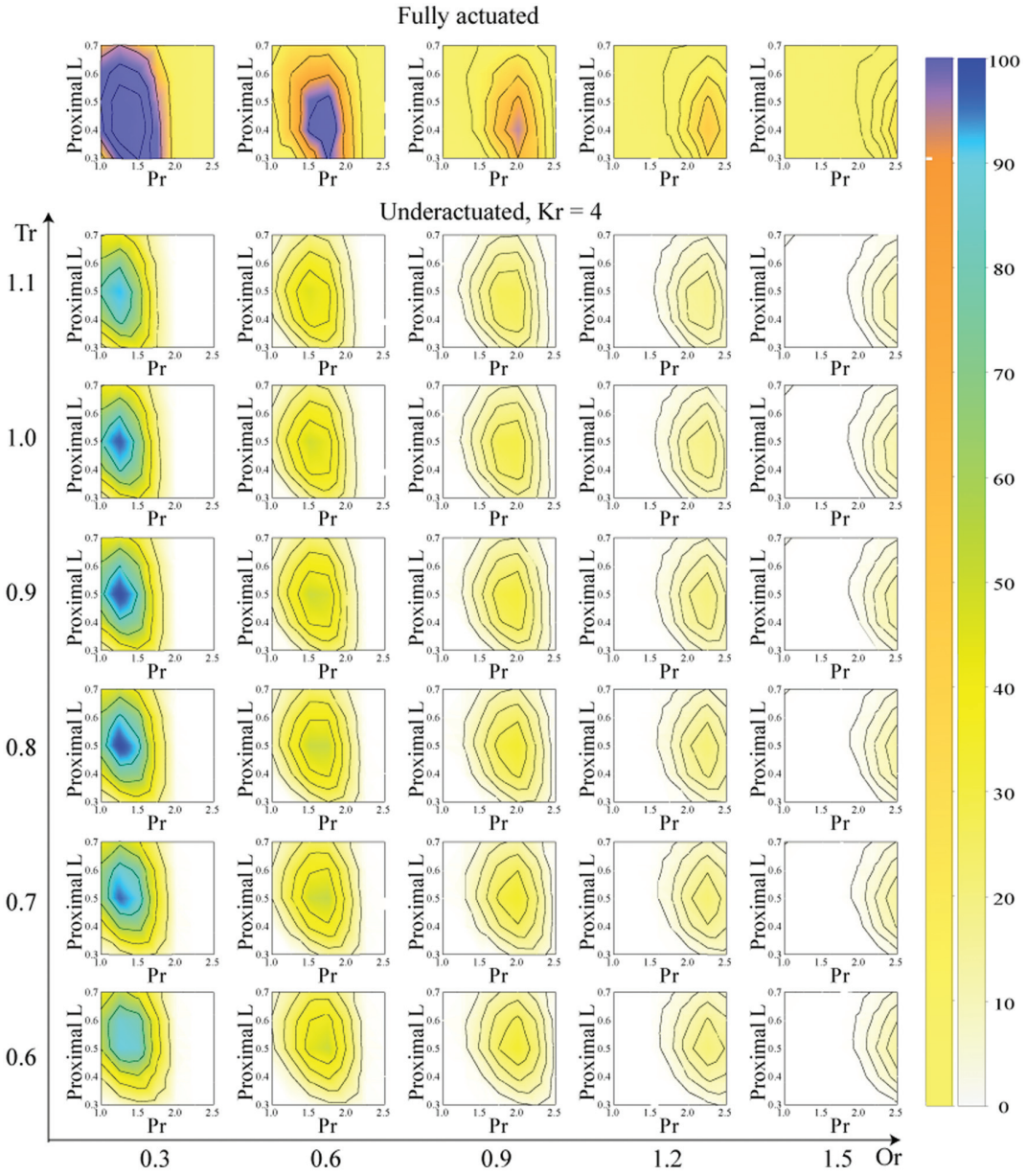

Fig. 6. Contour plots between proximal link length and palm size for growing size of the held object. The first row shows results of a fully actuated hand, following the first color bar code whose maximum value is 124,451 configurations. The rest of the rows show results for the under-actuated hand for the same object sizes and different values of transmission ratio from 0.6 to 1.1, following the second color bar code that reaches a maximum value in blue of 52,441 configurations.

As the object size is not a proper hand parameter, Figure 8 shows the same data set, plotting separetely the results for different sizes of the object, where the colors range again from 0 to 100, but they are scaled using the biggest size obtained for each object. The maximum workspace size in each plot compared to the overall maximal workspace is indicated at the top of each plot. Below each plot, we show a representation of the hand design that has the biggest workspace.

From Figure 8 we can observe several trends. For instance, the maximum size is always obtained at the maximum stiffness ratio. We analyze in depth this relationship in section 'On the stiffness constant'. Also, the optimal size of palm and object grow proportionally, at a ratio fairly constant of $P_r - O_r \approx 1$, that is, the radii difference between palm and object is about half of the length of the finger. The section 'On the palm size' will study this trend in detail.

5.1 On the stiffness constant

From the above simulation, we observed that the biggest workspace of the under-actuated hand is always obtained for the maximum stiffnes ratio possible.

Table 3. Geometrical parameters of the 10 biggest workspaces for a fully actuated hand and the maximum underactuated hand workspace achievable.

P_r	l	O_r	F-A	K_r	T_r	U-A	%
1.25	0.3	0.3	68,178	4	1.2	19,468	28.5
1.	0.5	0.3	74,928	4	1	40,623	54.2
1.5	0.6	0.3	75,709	4	0.6	40,253	53.2
1.75	0.4	0.6	78,652	4	0.9	23,749	30.2
1.25	0.6	0.3	87,001	4	0.7	44,462	51.1
1.5	0.3	0.3	101,191	4	1.1	20,639	20.4
1.5	0.5	0.3	108,369	4	0.7	45,456	41.9
1.25	0.5	0.3	117,999	4	0.8	52,441	44.4
1.25	0.4	0.3	122,914	4	1.1	41,859	34.1
1.5	0.4	0.3	124,451	4	0.8	36,035	28.9

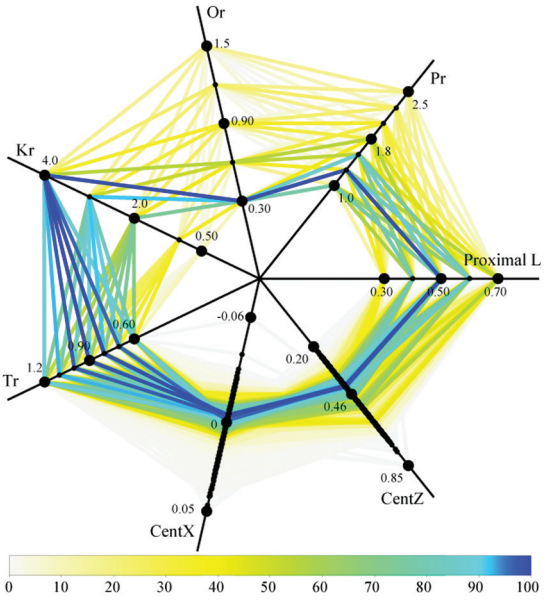

Fig. 7. Each polygon vertex lies on the axis of one of the parameters, at the length of the corresponding value of the parameter. The color of each polygon represents the size of the corresponding workspace for the under-actuated version of the hand.

To study this in detail we fixed all the parameters except the stiffness ratio, to $P_r = 1.2, DP_r = 1, O_r = 0.25$, $\alpha = 0.87, \beta = 1.04$ and $T_r = 0.8$. Then, we computed the size of fully actuated hand workspace and the size of the manipulation workspace of the under-actuated hand for growing values of K_r, from 4 to 70.

We found that the size of the manipulation workspaces of the under-actuated hand increases for bigger stiffness ratios, up to a maximum value which, for this particular design, was close to 50% of the workspace of the fully actuated hand. However, the magnitudes of the necessary actuation torques to obtain static equilibrium also grew.

Figure 9 shows the relationship between the median motor torque accross the workspace with the size of the workspace for different values of stiffness ratios. It can be observed how above $K_r = 8$, the size of the manipulation workspace can only grow a maximum of 2% more, but the values of the median actuation torques grow exponentially. Therefore, we need to chose a stiffness ratio as big as possible in accordance with the limiation of the motors of our hand.

We have also analyzed the location of the new configurations when the stiffness ratio grows. Our results indicated that the new configurations are always at the border of the workspace. In other words, when reducing the stiffness ratio to save motor enery, we will be only losing configurations away from the center position. Representations of the shape of the manipulation workspace can be found in the section 'Distribution of the Jacobian matrix indexes'.

5.2 On the palm size

From the results in Figure 7 we stated that the optimal relationship between size of palm and object was $P_r - O_r \approx 1$, that is, the difference between palm and object diameter similar to the length of the fingers. We study this relationship in more detail in Figure 10, where we can see the evolution of the contour plots between transmittion ratio vs. proximal link length for different sizes of palm and object for the under-actuated hand.

Looking at the axes $P_r - O_r$, we can see how the palm size increases in accordance with the object size, as we observed before. In addition, the optimal values are consistently obtained around a $DP_r = 1$, which corresponds to the proximal link length of 0.5. The transmission ratio slightly shifts from high values to lower values when the palm grows from small to big.

5.3 On the symmetry of the palm and the grasp

We performed a second execution, adding the parameters α and β to study the effect on the symmetry of the palm. Note that the variation of α changes the symmetry of the palm, whereas β changes the symmetry of the grasping points.

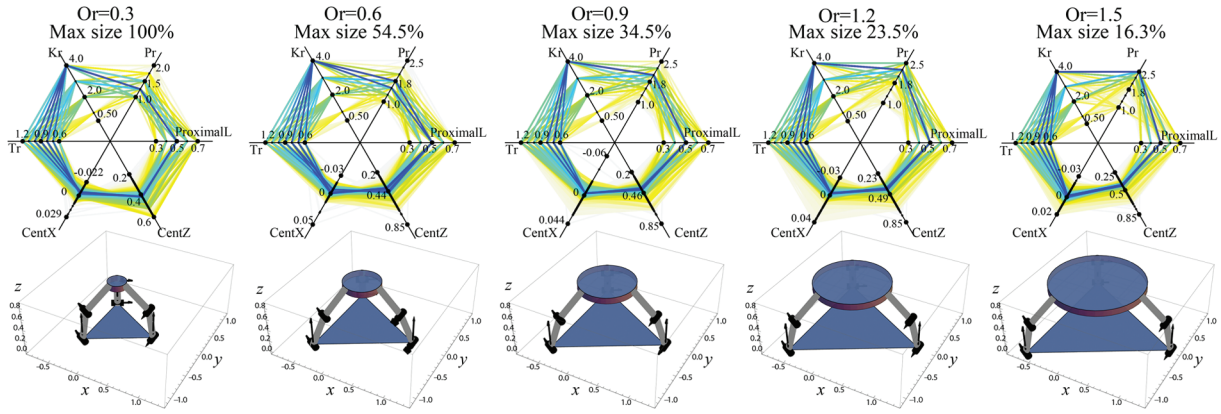

Fig. 8. The same set of data represented in Figure 7 here is separated into different object sizes. The colors are scaled depending on the maximum size for each object size. Below each plot, a representation is given of the under-actuated hand design using the parameters leading to bigger workspaces for each object size.

We have perfomed several executions exploring randomly the space of all the parameters using the ranges in Table 1. Our results indicated that the trends observed in the previous executions were mantained when adding these two extra parameters, but because of limitations on space, the results are not shown here. Then, we reduced the parameter space following the results obtained in the previous sections. That is, the size of palm and object grow accordingly, and so, we chose a fixed size object, and the corresponding optimal size of palm. Also, we can fix the value of the stiffness constant. Therefore, for the execution results shown next, we set $P_r = 1.5$, $O_r = 0.5$, and $K_r = 7$.

For the ranges and the step sizes shown in Table 4, we compute the sizes of the manipulation workspace for all possible combinations. This execution computes a total of 175 workspaces for fully actuated hands, and a total of 2,100 workpaces sizes for the under-actuated ones (that consider the extra parameter T_r).

The results of the fully actuated workspace can be seen in Table 5 and Figure 11. The table shows the best 2% sizes of fully actuated hand workspaces, with their corresponding maximum possible under-actuated hand workspaces. In the figure, we show the contour plots between α and β for different proximal link lengths. In this case, it is clear that the best results are obtained at the lower proximal link length and also at the diagonal $\alpha = \beta$, with slightly better results away from the symmetric configuraiton.

Table 5 shows, similarly as seen in Table 3, that the 2% maximum sizes for under-actuated workspace sizes correspond to different geometric parameters. The best size for the under-actuated hands ranges from 39, 057 to 38, 363, obtained with, respectively,

$$DP_r = 1, \alpha = \pi/3, \beta = \pi/3 \text{ and}$$

$$T_r = 0.95, 0.8, 0.9, 0.85$$

The results for the computation of under-actuated hand workspace sizes are shown in Figure 12. It is clear that all

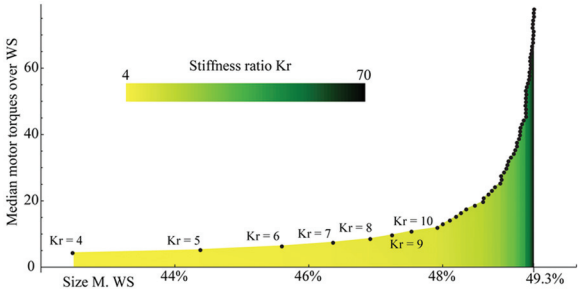

Fig. 9. Tradeoff between size of the manipulability workspace (that goes up to 49% of the kinematic workspace) versus motor torque values, that grows linearly with the value of K_r.

Table 4. Range of values of the parameters for the results in Figures 11 and 12.

Parameter	Range	Step
P_r	1.5	–
l	$(0.4, 0.7)$	0.05
O_r	0.5	–
α	$(0.84, 1.25)$	$\pi/30$
β	$(0.84, 1.25)$	$\pi/30$
K_r	7	–
T_r	$(0.5, 1.3), (0.85, 1.05)$	0.1,0.05

of the optimal sizes are obtained in the diagonal $\alpha = \beta$, being the best one the central one, corresponding to the symmetric hand. Observe also that the pattern for the relationship betweeen T_r and DP_r is fairly constant in all the plots, indicating that is not affected by the parameters α and β, with the biggest size between the values $T_r \in (0.8, 1)$ and DP_r around 1.

5.4 Distribution of the Jacobian matrix indexes

To study the quality of the grasp, the grasping literature typically uses different indexes related to the Jacobian

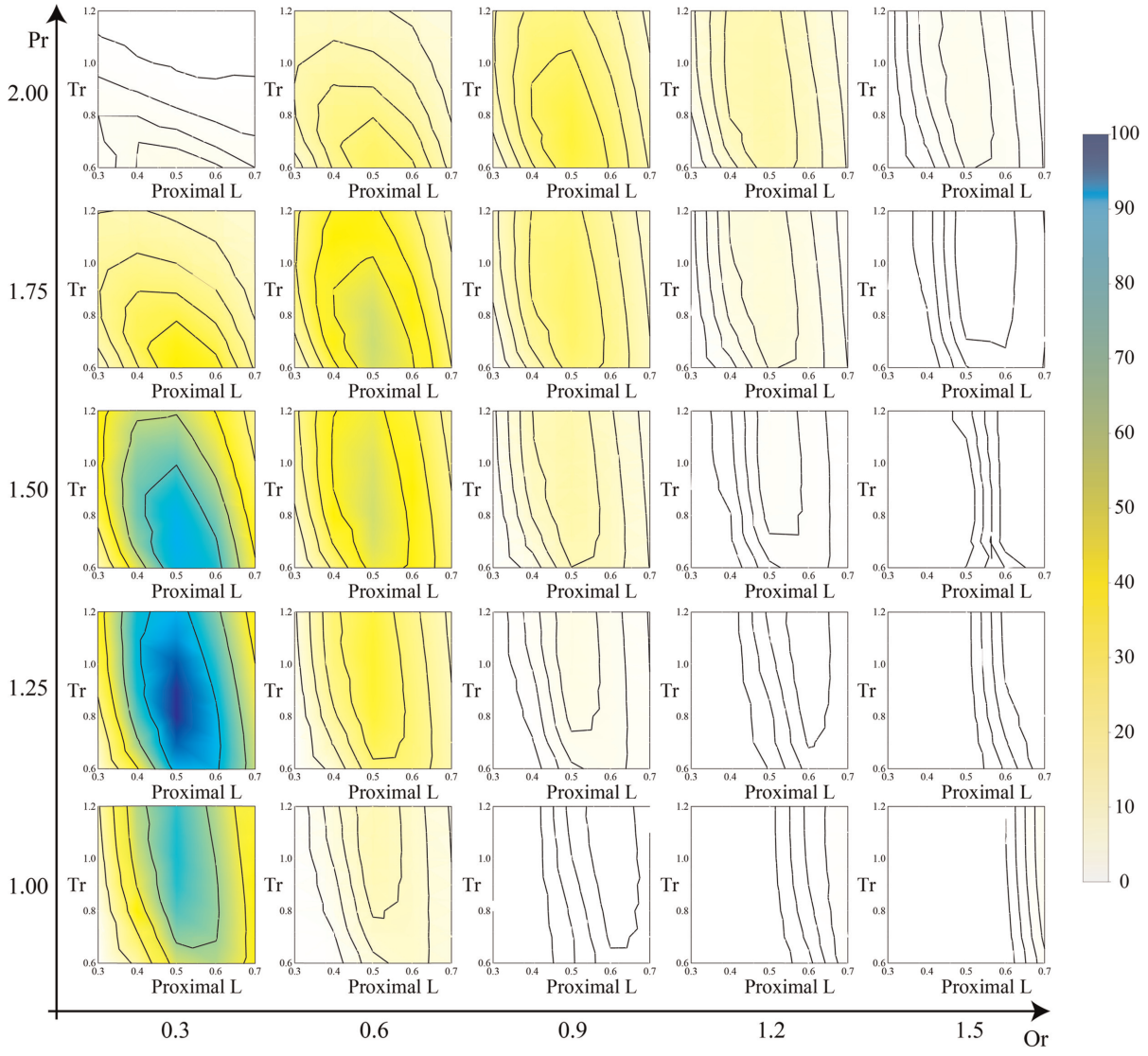

Fig. 10. Evolution of the size of the workspaces for under-actuated hands. We show contour plots between transmission ratio and proximal link lengths across different palm and object sizes, with the rest of the parameters fixed to $\alpha = \beta = \pi/3$ and $K_r = 4$.

Table 5. Best fully actuated workspaces for $P_r = 1.5$ and $O_r = 0.5$.

Prox L	α	β	F-A	T_r	U-A
0.45	1.25	1.24	93908	0.9	33961
0.45	0.84	0.84	94355	0.9	32387
0.4	1.26	1.24	94827	1.	28361
0.4	0.84	0.84	95097	0.95	26558

matrix of the system. Sometimes this relates only to the Grasp matrix, and sometimes it relates to the combination of both the Grasp matrix and the hand Jacobian (Shimoga, 1996). From our analysis, we want to study how these values look for one hand plus object with optimal workspace size. We have chosen the parameters

$$P_r = 1.5, DP_r = 1, O_r = 0.5, \alpha = \pi/3, \beta = \pi/3,$$

$$K_r = 7, T_r = 0.9,$$

that lead to a fully actuated hand with 83, 566 configurations workspace and a under-actuated version with 38, 749 (that is a 46.4%).

The most widely used index is the condition number of the matrix $\boldsymbol{J}^T$ (Merlet, 2006b), which is valid for both under-actuated and fully actuated hands, and is defined as

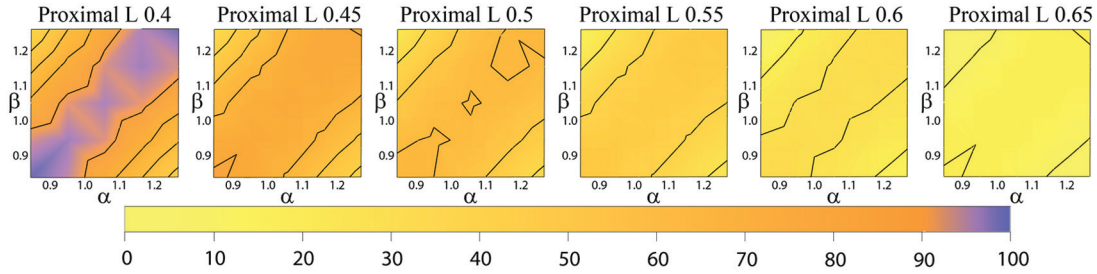

Fig. 11. Sizes of a fully actuated version of the hand for different proximal link lengths when the symmetry at the palm and at the contact points changes, also for a fixed palm and object of $P_r = 1.5$, object to $O_r = 0.5$.

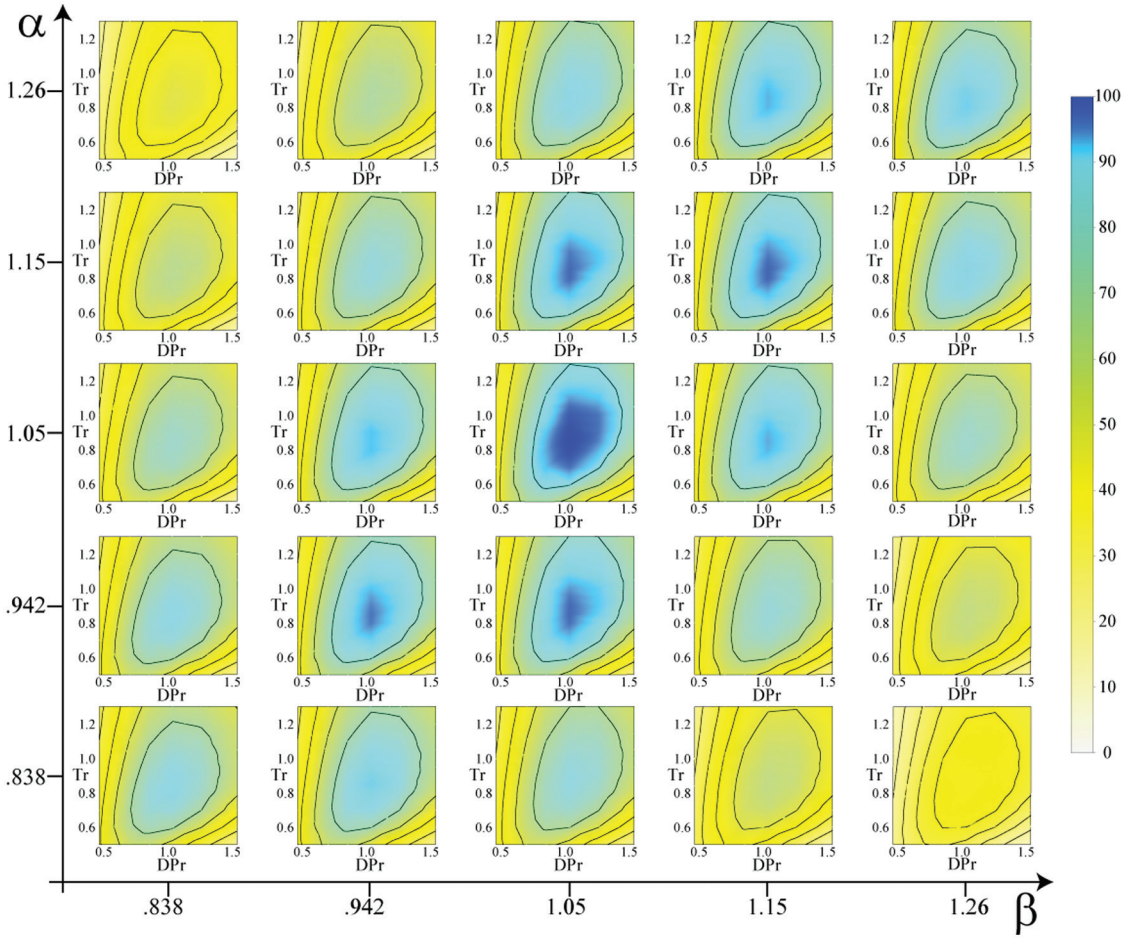

Fig. 12. Graphic of contour plots for different symmetry parameters α and β, for a palm ratio fixed to $P_r = 1.5$, object to $O_r = 0.5$ and $K_r = 7$.

$$\kappa(\boldsymbol{J}^T) = \frac{Max\left[Eigenvalues\left(\boldsymbol{J}^T\boldsymbol{J}\right)\right]}{Min\left[Eigenvalues\left(\boldsymbol{J}^T\boldsymbol{J}\right)\right]}$$

Note that the condition number ranges from 1 to ∞, optimal being 1.

However, the matrix that defines the singularities of the static equilibrium equations in the under-actuated case is the reduced $\boldsymbol{J}_a$ matrix, which depends on the geometrical parameters and on the transmission ratio T_r. The determinant of $\boldsymbol{J}_a$ gives us an idea of the magnification of the actuation torques for a given external force. For a configuration where its value is close to zero, small external forces may need very big actuation torques to achieve equilibrium. These kinds of configurations are called type 2 singularities (Gosselin and Angeles, 1990).

Figure 13 shows a representation of the position workspace for the fully actuated (black) and the under-actuated workspaces (colored) of the same hand. In Figure 13(left),

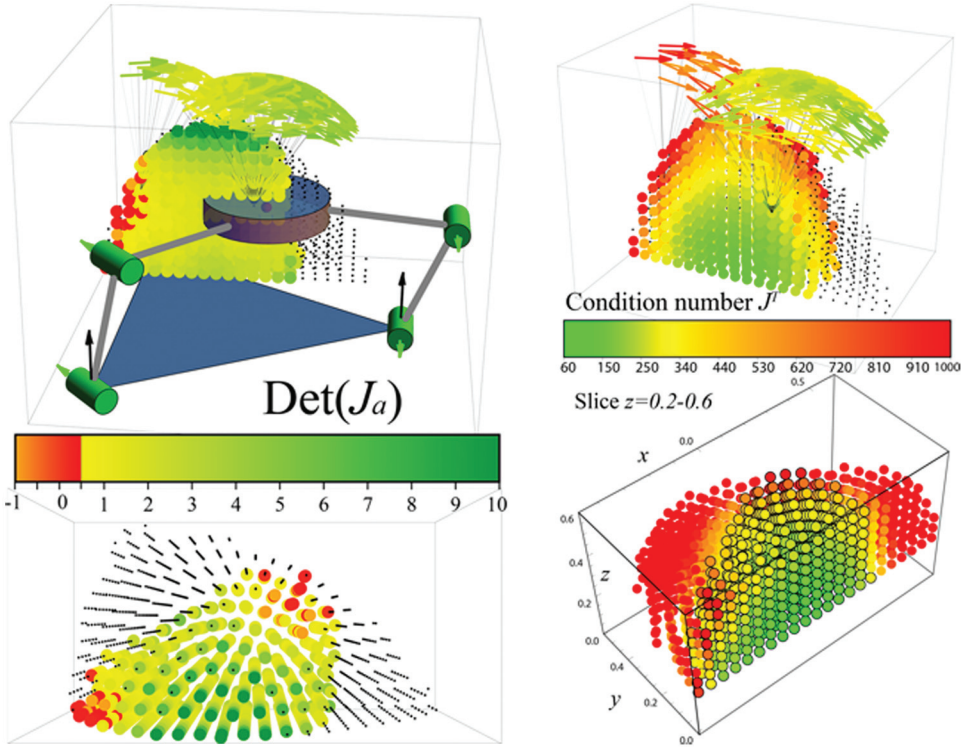

Fig. 13. Evolution of the determinant of the Jacobian matrix and the condition number for the workspace of a hand with parameters $P_r - 1.5$, $DP_r = 1$, $O_r = 0.5$, $\alpha = \pi/3$, $\beta = \pi/3$, $K_r = 7$, and $T_r = 0.9$.

each dot color represents the minimum value of $Det(\boldsymbol{J}_a)$ in all the orientations achievable from the dot position. In Figure 13(right), each dot color represents the median value of the condition number of $\boldsymbol{J}^T$ in all the orientations achievable from the dot position. The bottom (right) figure shows a piece of the fully actuated hand workspace, bordering in black the positions that are also inside the under-actuated workspace.

We can observe that the determinant of the matrix $\boldsymbol{J}_a$ is bigger than 0.5 in almost all the workspace, being closer to singularity at the border of the workspace. Further analysis is needed to know where the second type of singularities is located (Gosselin and Angeles, 1990), but preliminary results show that the more optimal workspaces are those where these type of singularities occur outside the reachable workspace.

We can also see in Figure 13 (bottom right) that the configurations that belong to the under-actuated workspace are the ones with lower condition number.

6. Conclusions

This work uses a framework for robotic hands inspired in the parallel robots literature that computes the manipulation workspace of a hand-plus-object system. This allows us to explore the space of design parameters to find the hand geometry that maximizes the size of the manipulation workspace.

Our computations assume that the normals to the object surface at the contact points are directed towards the center of mass. This covers round shapes including spherical and disk objects, which are the most commonly grasped with the tripod grasp. In addition, we modeled the contact points using the point with friction model, and thus, may not be accurate away from the initial central position $(p_x, p_y) = (0, 0)$. To take that into account, we impose a minimum angle of 120° between the normal to the surface of the object at the contact point and the contact phalange.

Without taking into account the limitations on the motors, we have observed that using under-actuation can decrease the size of the manipulation workspace significantly up to 80%. However, an optimal choice of the under-actuation parameters can lead to a reduction of only 50% of the fully actuated hand workspace. More importantly, the 50% of the workspace that belongs to the under-actuated hand workspace is always located at the center of the object with respect to the hand, which are the most relevant in practice.

Our design parameters exploration has shown several additional interesting results. The diameter of the palm and the diameter of the object are optimal when $P_r - O_r \approx 1$, which means that the radii difference is about half of the length of the finger. Note that for $P_r = O_r$ the fingers are in a singularity at any central configuration $(p_x, p_y) = (0, 0)$, because the fingertip lies in the same (x, y) coordinates that the base of the finger, allowing the rotation of the first joint

without modifying the location of the fingertip. Therefore, it makes sense that the optimum is as far away as possible from being in a singular configuration at the center of the workspace, without being at a distance that disables mobility. Future work will study if such results are valid when using the antropomorphic adbduction/adduction axis instead of the vertial one in the fingers. However, for all the existing robotic hands using the verital axis, the design of the palm should have a diameter equal to the mean size of object sizes we want to manipulate plus 1, so that they work as well as possible with a wide range of object sizes.

Our results also show that the distal–proximal ratio seems to be optimal when it is close to 1 (for under-actauted) or slightly bigger than 1 (for fully actuated). The ratios that are usually seen in most of two-link finger hands are smaller than 1, meaning a shorter distal link. This is because dimensional synthesis applied to single fingers shows optimal conditioning at 0.7071 (Salisbury and Craig, 1982), whereas Yoshikawa (1985) obtained optimal manipulability and finger workspace volume at a ratio of 1. However, these are results optimizing single fingers, and not the workspace obtained with the combination of all of them. It was expected that our results could indicate slightly different results to optimize manipulation workspace size. Note that if you consider a typical three-link anthropomorphic finger with the distal joint locked, the ratio between the two distal links and the proximal is closer or even slightly bigger than 1. This indicates that the tripod grasp with the antropomorphic three-linked fingers is already optimized for workspace size, even if the distal joint is kept fixed.

Our results also show that more optimal workspaces with the tripod grasp are obtained for symmetric placement of the fingers in the hand when the hand is under-actuated. Regardless, we have seen that whatever the distribution on the palm, it is best to use the same distribution for the grasp contact points both for the under-actuated and for fully actuated hands. However, this result may be different if we change our assumption on the normal to the object surface pointing towards the center of mass.

We have also shown that, for under-actuated hands, increasing the finger stiffness ratio also increases the workspace, at the cost of requiring larger actuation torques.

The optimal transmission ratios were found around 0.9, decreasing slightly for bigger palm sizes independently of the distal–proximal ratio.

The results presented in this paper are valid for the studied three-fingered hand structure using a fully actuated hand versus an under-actuated version of the same hand design. More generally, we can state that the optimal dimensions to obtain big manipulation workspaces are different from others obtained optimizing a single grasp. For instance, for manipulation workspaces, robotic hands seem to need bigger distal–proximal ratios and bigger palms than the ones seen in commercial hands such as the Barret hand or the Schunk SDH hand. Additional analysis would be needed to extend these results to other hand configurations, including allowing the thumb to have a different geometry as well as the analysis of three link fingers as in anthropomorphic configurations.

Optimal design for robotic hands is a challenging problem where many considerations need to be taken into account. A design process usually involves optimization of several criteria. We have shown that manipulation workspace size is a relevant criterion to consider, particularly for under-actuated hands, to avoid significant reductions of workspace that can greatly limit the versatility of the final hand design.

Funding

This work was supported in part by a grant from the National Science Foundation, grant NSF IIS-0953856.

References

Balasubramanian R, Belter J and Dollar A (2012) Disturbance response of two-link underactuated serial-link chains. *Journal of Mechanisms and Robotics* 4: 021013.

Bicchi A and Prattichizzo D (2000) Manipulability of cooperating robots with unactuated joints and closed-chain mechanisms. *IEEE Transactions on Robotics and Automation* 16: 336–345.

Borràs J and Dollar A (2013a) Framework comparison between a multifingered hand and a parallel manipulator. In: *Computational kinematics* (eds F Thomas and AP Gracia), Barcelona, Spain, pp. 219–227. Springer.

Borràs J and Dollar A (2013b) A parallel robots framework to study precision grasping and dexterous manipulation. In: *IEEE international conference on robotics and automation*, Karlsruhe, Germany, pp. 1595–1601. IEEE.

Borràs J and Dollar A (2014) Analyzing dexterous hands using a parallel robots framework. *Autonomous Robots* 36: 169–180.

Bullock I, Ma R and Dollar A (2012a) A hand-centric classification of human and robot dexterous manipulation. *IEEE Transactions on Haptics* 6: 129–144.

Bullock I, Borràs J and Dollar A (2012b) Assessing assumptions in kinematic hand models: a review. In *IEEE Ras/Embs International conference on biomedical robotics and biomechatronics*, Rome, Italy, 24–27 June, pp. 139–146. IEEE.

Bullock I, Feix T and Dollar A (2013) Finding small, versatile sets of human grasps to span common objects. In *IEEE international conference on robotics and automation*, Karlsruhe, Germany, 6–10 May, pp. 1068–1075. IEEE.

Butterfaß J, Grebenstein M, Liu H, et al. (2001) Dlr-Hand Ii: Next generation of a dextrous robot hand. In *IEEE international conference on robotics and automation (ICRA)*, vol. 1, Seoul, South Korea, 21–26 May, pp. 109–114. IEEE.

Butterfaß J, Hirzinger G, Knoch S, et al. (1998) Dlr's multisensory articulated hand. I. Hard-and software architecture. In *Proceedings of IEEE international conference on robotics and automation*, vol. 3, Leuven, Belgium, 16–20 May, pp. 2081–2086. IEEE.

Ciocarlie M and Allen P (2011) A constrained optimization framework for compliant underactuated grasping. *Mechanical Sciences* 2: 17–26.

Ciocarlie M, Hicks F and Stanford S (2013) Kinetic and dimensional optimization for a tendon-driven gripper. In *IEEE*

international conference on robotics and automation, Karlsruhe, Germany, 6–10 May pp. 2751–2758. IEEE.

Cui L and Dai J (2012) Reciprocity-based singular value decomposition for inverse kinematic analysis of the metamorphic multifingered hand. *Journal of Mechanisms and Robotics* 4: 034502.

Cutkosky M (1989) On grasp choice, grasp models, and the design of hands for manufacturing tasks. *IEEE Transactions on Robotics and Automation* 5(3): 269–279.

Dai J and Wang D (2007) Geometric analysis and synthesis of the metamorphic robotic hand. *Journal of Mechanical Design* 129: 1191.

Dai J, Wang D and Cui L (2009) Orientation and workspace analysis of the multifingered metamorphic hand—metahand. *IEEE Transactions on Robotics* 25: 942–947.

Das I and Dennis J (1997) A closer look at drawbacks of minimizing weighted sums of objectives for pareto set generation in multicriteria optimization problems. *Structural Optimization* 14: 63–69.

Dollar A and Howe R (2010) The highly adaptive sdm hand: design and performance evaluation. *The International Journal of Robotics Research* 29: 585–597.

Gosselin C and Angeles J (1990) Singularity analysis of closed-loop kinematic chains. *IEEE Transactions on Robotics and Automation* 6: 281–290.

Grebenstein M, Albu-Schaffer A, Bahls T, et al. (2011) The Dlr hand arm system. In: *IEEE international conference on robotics and automation (ICRA)*, Shanghai, China, 9–13 May, pp. 3175–3182. IEEE.

Grebenstein M, Chalon M, Hirzinger G, et al. (2010) A method for hand kinematics designers. 7 Billion perfect hands. In: *International conference on applied bionics and biomechanics*, Venice, Italy, 14–16 October.

Hammond Fl, Weisz J, De La Llera Kurth A, et al. (2012) Towards a design optimization method for reducing the mechanical complexity of underactuated robotic hands. In *IEEE International conference on robotics and automation (ICRA)*, Saint Paul, USA, 14–18 May, pp. 2843–2850. IEEE.

Jacobsen S, Iversen E, Knutti D, et al. (1986) Design of the utah/mit dextrous hand. In: *IEEE international conference on robotics and automation*, vol. 3, pp. 1520–1532. IEEE.

Kerr J and Roth B (1986) Analysis of multifingered hands. *The International Journal Of Robotics Research* 4: 3–17.

Martell J and Gini G (2007) Robotic hands: Design review and proposal of new design process. *Proceedings of World Academy of Science, Engineering and Technology* 20: 85–90.

Mason M and Salisbury J (1985) *Robot Hands and the Mechanics of Manipulation*. Cambridge, MA: MIT Press.

Mason M, Srinivasa S and Vazquez A (2011) Generality and simple hands. *Robotics Research. Springer Tracts in Advanced Robotics*. Berlin Heidelberg: Springer, pp. 345–361.

Matsuoka Y, Afshar P and Oh M (2006) On the design of robotic hands for brain-machine interface. *Neurosurgical Focus* 20: 1–9.

Merlet J (2006a) *Parallel Robots*. 2nd ed. Dordrecht: pp. 301–320.

Merlet J (2006b) Jacobian, manipulability, condition number, and accuracy of parallel robots. *Journal of Mechanical Design* 128: 199–206.

Michelman P (1998) Precision object manipulation with a multifingered robot hand. *IEEE Transactions on Robotics and Automation* 14: 105–113.

Mohamed M and Duffy J (1985) A direct determination of the instantaneous kinematics of fully parallel robot manipulators. *Journal of Mechanisms Transmissions and Automation in Design* 107: 226–229.

Odhner L and Dollar A (2011) Dexterous Manipulation with underactuated elastic hands. In *IEEE International conference on robotics and automation*, Shanghai, China, 9–13 May, pp. 5254–5260. IEEE.

Odhner L, Jentoft L, Claffee M, et al. (2013) A compliant, underactuated hand for robust manipulation. *The International Journal of Robotics Research* 33: 736–752.

Okada T (1982) Computer control of multijointed finger system for precise object-handling. *IEEE Transactions on Systems, Man and Cybernetics* 12: 289–299.

Salisbury J and Craig J (1982) Articulated hands: Force control and kinematic issues. *The International Journal Of Robotics Research* 1: 4–17.

Schunk (2013) *Schunk Dextrous Hand Sdh*. Available at: www.Schunk.Com (accessed 8 October 2015).

Shimoga K (1996) Robot grasp synthesis algorithms: A survey. *The International Journal of Robotics Research* 15: 230–266.

Simo-Serra E, Perez-Gracia A, Moon H, et al. (2012) Kinematic synthesis of multi-fingered robotic hands for finite and infinitesimal tasks. *Latest Advances In Robot Kinematics*. Dordrecht: Springer, pp. 173–180.

Townsend W (2000) The Barretthand grasper – programmably flexible part handling and assembly. *Industrial Robot: An International Journal* 27: 181–188.

Tsai L-W (1999) *Robot Analysis. The Mechanics of Serial and Parallel Manipulators*. New York: John Wiley & Sons, Inc.

Yoshikawa T (1985) Manipulability of robotic mechanisms. *The International Journal of Robotics Research* 4: 3–9.